Rheo-SAXS study of a shear-thinning hydrogel containing clay nanoplatelets

Claire Hotton, Guylaine Ducouret, Juliette Sirieix-Plénet, Thomas Bizien, Clément Guibert, Pierre Levitz, Laurent Michot, Natalie Malikova

Rheo-SAXS study of a shear-thinning hydrogel containing clay nanoplatelets

Claire Hotton[a], Guylaine Ducouret[b], Juliette Sirieix-Plénet[a], Thomas Bizien[c], Clément Guibert[d], Pierre Levitz[a], Laurent Michot[a], Natalie Malikova[a,*]

[a]*Laboratory of Physical Chemistry of Electrolytes and Interfacial Nanosystems (PHENIX), Sorbonne Université, CNRS, 75005 Paris, France*
[b]*Laboratory of Soft Matter Sciences and Engineering (SIMM), ESPCI Paris, PSL Research University, Sorbonne University, CNRS, F-75005 Paris, France*
[c]*Synchrotron SOLEIL, l'Orme des Merisiers, Saint-Aubin - BP 48, 91192 Gif-sur-Yvette CEDEX, France*
[d]*Surface Reactivity Laboratory (LRS), Sorbonne Université, CNRS, 75005 Paris, France*

Abstract

Shear-induced orientation of clay nanoplatelets within a physically cross-linked hydrogel based on ionenes, positively charged polyelectrolytes, is studied here. Small angle X-ray scattering measurements (SAXS) are performed under shear within a Couette cell cylinder (rheo-SAXS). As the SAXS signal is dominated by that of the clay component, we follow the evolution of the orientational distribution of the clay nanoplatelets within the hydrogel as a function of shear. We investigate the effect of the clay volume fraction, polyelectrolyte concentration, clay charge location and clay charge density by screening three different types of clay: Wyoming and Arizona montmorillonites and Idaho beidellite. The orientational field of clay nanoplatelets in the gel is shown to strongly depend on the clay charge location and shear rate, whereas it is independent of the clay volume fraction. Approaching the critical gelation concentration of the polyelectrolyte system, these features change drastically.

Keywords: Clay nanoplatelets, Hydrogel, Particle orientation, Polyelectrolyte, Rheo-SAXS

1. Introduction

Clay-containing hydrogels are promising materials as the interaction between polymer and clay leads to enhanced mechanical (Takeno and Nagai, 2018; Chang et al., 2010), thermal (Zhao et al., 2015), swelling (Darvishi et al., 2011) or barrier properties (Jesus et al., 2018). This allows them to have numerous applications especially in the biomedical fields where they can be used as scaffolds for tissue regeneration, implants or biosensors (Davern et al., 2024; Yang et al., 2023; Leu Alexa et al., 2021; Murugesan and Scheibel, 2020). Moreover, the shear-thinning behaviour of clay-based hydrogel as well as the possibility of tuning the orientation of clay nanoplatelets to modify the permeation properties of the hydrogel, allows them to act as an efficient injectable drug-delivery system (Sheikhi et al., 2018). For this purpose, it is relevant to establish the parameters that may influence the clay orientation inside the hydrogel. In this study, we investigate the orientation of clay platelets under shear in a physically cross-linked hydrogel. This hydrogel is formed from cationic polyelectrolytes based on ionenes, a class of polyelectrolytes containing quaternary ammonium parts in the main chain (Noguchi, 1972; Misawa et al., 2008; Hotton et al., 2021). Additionally, the presence in the main chain of aromatic rings and amide moities allows gelation through a combination of electrostatic repulsions, π-π stacking, hydrogen bonding and anion-π and cation-π interactions that can be tune according to the nature and the valence of the couterions (Hotton et al., 2023).

In a previous study, we investigated the organisation of clay nanoplatelets in this ionene-based hydrogel (Hotton et al., 2021). We have brought to light that clay nanoplatelets present a local lamellar order within the gel. First, this ordering is mediated by the polyelectrolyte network and is independent of the clay volume fraction. Then, the degree of ordering of the system, as well as the mechanical properties of the hydrogel, is sensitive to the exact negative clay charge location and clay charge density. In this study, we aim to probe the shear-induced orientation as a function of the clay type, clay volume fraction and polyelectrolyte concentration. Using different types of clay enable to study the effect of different clay charge densities and clay charge locations.

In the case of pure clay samples, by coupling rheology experiments performed in a Couette cell with small angle X-ray scattering (rheo-SAXS) some of us showed in the past (Philippe et al., 2011),(Philippe et al., 2013) that the shear thinning behaviour of aqueous clay suspensions was directly linked to the orientational features of the individual platelets. A strong influence of clay type was also evidenced in these studies. It is therefore relevant to anal-

*Corresponding author
Email address: natalie.malikova@sorbonne-universite.fr (Natalie Malikova)

yse, using rheo-SAXS, if the tendencies observed for pure clay aqueous suspensions hold, once they are incorporated inside a hydrogel. In particular, it appears fruitful to determine if the orientational field of clay platelets can be directly linked to the shear-thinning behaviour of hydrogel and thus to assess to what extent the clay particles and their nature controls the rheological behaviour of the gel containing them.

2. Experimental section

2.1. 6-Cl modified ionene and precursor synthesis

The cationic polyelectrolyte used in this study is an ionene referred to 6-Cl modified ionene (6-Cl) ((Supplementary Material S1). The 6-Cl and its precursor were synthesized via a two-step reaction according to a protocol already described in a previous article (Hotton et al., 2021). All chemical reagents were purchased from Sigma-Aldrich and used without further purification. All solvents were purchased from Sigma-Aldrich and VWR.

2.1.1. First step: synthesis of 1,4-bis-[4-(chloromethyl)benzamido]benzene

All vials used were dried in an oven at 80°C the day before. *p*-phenylenediamine (1.08 g, 10 mmol, 1 eq) was dissolved in freshly distilled dichloromethane (100 mL) into a 250 mL round-bottom flask with a magnetic stirrer and placed under an inert argon atmosphere. The solution in the round-bottom flask was then cooled to 0°C by using an ice-water bath and triethylamine (3.5 mL, 25 mmol, 2.5 eq) was added. A solution of 4-(chloromethyl)benzoyl chloride (3.78 g, 20 mmol, 2 eq) dissolved in distilled dichloromethane (70 mL) was added dropwise with an isobar dropping funnel. After the addition, the ice-water bath was removed, and the system was warmed up to room temperature. The system was stirred for 24h to ensure complete conversion. The obtained white precipitate was vacuum filtrated and then washed with distilled water (2 x 80 mL). The product was dried under vacuum at 90°C. The product was obtained in high yield (85%). Structural analysis was carried out by ^{1}H-NMR in DMSO-d_6.

2.1.2. Second step: synthesis of 6-Cl modified ionene

1,4-bis-[4-(chloromethyl)benzamido]benzene (2.06 g, 5 mmol) was dissolved in dimethylformamide (200 mL) at 80°C in a 500 mL round-bottom flask with a magnetic stirrer. Then, N,N,N',N'-tetramethyl-1,6-hexanediamine (1.07 mL, 5 mmol) was added. The system was stirred at 80°C for 48h. The obtained yellow precipitate was vacuum filtrated and washed subsequently with dimethylformamide (100 mL), acetonitrile (100 mL) and dichloromethane (100 mL). The product was dried under vacuum at 50°C. The 6-Cl modified ionene was obtained in good yield (75%). Structural analysis was carried out by ^{1}H-NMR in D_2O. The average molecular weight of the 6-Cl modified ionene was previously determined as 7.84 10^4 Da (Misawa et al., 2008).

2.2. Clay fraction, purification and cations exchange

Three different clay minerals (two Na-montmorillonites, Arizona (SAz-1) and Wyoming (SWy-2), and a Na-beidellite from Idaho (BId)) were purchased from the Source Clays Minerals Repository of the Clay Mineral Society at Purdue University, Indiana. Clay suspensions were purified and separated in size fractions by successive centrifugation following the previously established procedure (Paineau et al., 2011; Michot et al., 2004). Each fraction has a defined average platelet size with a reduced size polydispersity. Here we used one size fraction denoted T3 for all clays. The characteristic sizes and the cation-exchange capacities related to the charge densities of the clay particles we are interested in are summarized in Table 1 (Paineau et al., 2011). The BId is a tetrahedrally substituted clay whereas the SAz-1 and the SWy-2 are octahedrally subtituted clays.

Table 1: Main features of different clay particles used in this study: the lateral dimension D, the polydispersity in diameter, the average thickness e and the cation-exchange capacity (CEC). All systems were used with Na as the compensating counterion.

	SAz-1	SWy-2	BId
D (nm)	95	100	209
Polydispersity (%)	19	25	38
e (nm)	0.7	0.7	1
CEC (mmol/100g)	122.5	96.4	94.3

2.3. Preparation of the 6-Cl/clay hydrogels

The 6-Cl was first added into a clay suspension and dispersed by using a sonicator (Fisher Scientific FB 15051) for 15 minutes. Then the mixture was heated at 70°C for 10 minutes followed by cooling to room temperature to form the hydrogel. The sonication step was seen as essential for producing visually transparent gels. The critical gelation concentration (CGC) was determined to be around 10 g/L via vial inversion method and rheology measurements.

2.4. Viscosity measurements

The rheo-SAXS experiments were performed with an Anton Paar MCR-501 imposed stress rheometer equipped with a Couette cell at 25°C. The Couette geometry consisted of two co-axial cylinders: a static outer cylinder (the stator) and a rotating inner cylinder (the rotor). The external R_{ext} radius of the stator and the internal radius of the rotor R_{in} were 10.25 mm and 9.75 mm respectively. Thus we had a gap of 500 μm and a total immersed volume height of 17 mm. The Couette cell was made of polycarbonate in order to limit the X-ray absorption by the cell. The samples were prepared several days before the experiment. After introduction of the sample into the rheometer, a shear rise from 100 s^{-1} to 5000 s^{-1} in 145 seconds and a 2-minute pre-shear at 5000 s^{-1} was applied. The sample

was then left at rest for 3 minutes. This pre-shear was necessary to remove the history of the sample and to have the same initial state for each sample before the measurement. The flow measurements were then carried out from 5000 s^{-1} to 1 s^{-1}. In preliminary measurements, we found that when a constant shear rate was applied to the sample over time, the viscosity decreased for 1 minute and then stabilised and reached a plateau. The samples were therefore sheared for 5 minutes at each shear rate during the experiment to ensure that this plateau was reached prior to the SAXS measurement. The flow curves presented here correspond to the measurements made during the ramp of decreasing shear rates.

2.5. Small Angle X-ray Scattering (SAXS)

Rheo-SAXS experiments were conducted at the SWING beamline of the SOLEIL synchrotron (Orsay, France) using a fixed incident energy of 12 keV with one sample-to-detector distance of 1.5 m. Thus the q range available, q being the scattering wavevector, was 0.006 $Å^{-1}$ < q < 0.6 $Å^{-1}$. The rheometer described above was implemented on the beamline to measure the scattered intensity under shear and several studies have already benefitted from this so-called rheo-SAXS set-up (Bihannic et al., 2010; Philippe et al., 2011, 2012, 2013). For each sample, the scattered intensity was measured at different shear rates from 5000 s^{-1} to rest. The system was kept at the same shear rate for 5 minutes. After 1 minute of shear, the viscosity plateau was reached. Thereafter an average over 50 acquisitions (over 5 minutes of total duration) was made to achieve good statistics. For each sample and shear rate, the scattered intensity was measured at two different positions within the Couette geometry: in radial and tangential position. These two different positions are shown in Figure 1. In the radial position, the incident beam is perpendicular to the streamlines, also called velocity lines. In the tangential position, the incident beam passes through the Couette cell in the direction of flow, i.e. parallel to the streamlines.

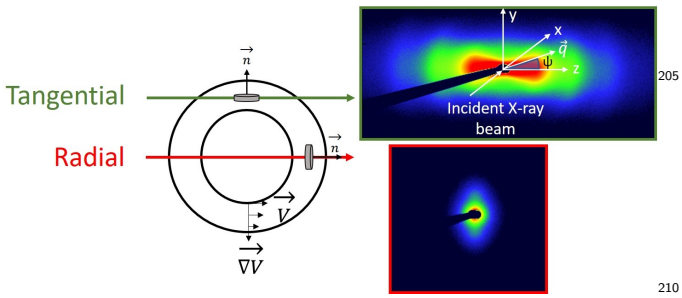

Figure 1: Cross-section of the Couette geometry. 2D SAXS images obtained, under a shear of 3000 s^{-1}, in the tangential position (green) and in the radial position (red) for 30 g/L 6-Cl gel with 0.15% BId-T3-Na. The vectors represent the velocity lines and the velocity gradient. In the scattering image in the tangential position, the detector reference frame is depicted, showing the angle representing the orientation of the scattering vector, $\vec{q}$, in the plane of the detector (zx plane) and the beam arriving along the y direction.

3. Results and discussion

3.1. Analysis of 2D scattering patterns

Two-dimensional scattering patterns were recorded on an Eiger 4M (Dectris) detector. An example of the scattering 2D patterns obtained for 30 g/L 6-Cl gel with 0.15% BId-T3-Na at different shear rates, in the radial and tangential positions is given in Figure 2.

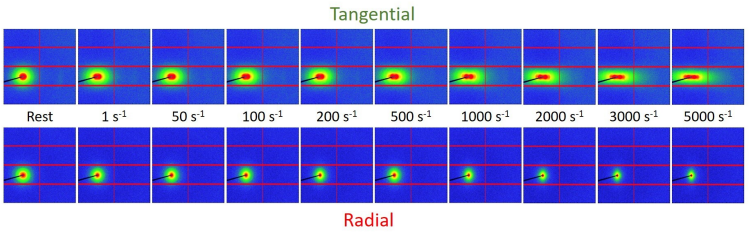

Figure 2: SAXS 2D patterns recorded for a 30 g/L 6-Cl gel with 0.15% BId-T3-Na at different shear rates, in the radial and tangential positions, as indicated. The red grid in each pattern corresponds to the boundaries between the different parts of the Dectris detector.

To analyse the anisotropy of the 2D images and thus determine the orientation field of the clay platelets within the gel, we analyse the scattered intensity as a function of the angle ψ for a fixed scattering wavevector value q. In fact, to study the orientation of the platelets, we study the orientation distribution function (PDF or probability density function) of the vector normal to the surface of a platelet, shown in the shear reference frame (Jeffery and Filon, 1922; Bihannic et al., 2010; Philippe et al., 2013), as depicted in Figure 3 (A). The normal vector is defined in the shear reference frame by a polar angle θ and an azimuthal angle ϕ. The statistical confinement of the normal vector to the platelet under shear describes an ellipsoid (Bihannic et al., 2010; Baravian et al., 2010; Michot et al., 2009), as shown in Figure 3 (B). Taking this description into account, we can write the PDF as (Bihannic et al., 2010) :

$$PDF(\theta,\phi) = \frac{a_x a_y a_z}{4\pi} \frac{1}{((a_x^2 cos^2\phi + a_y^2 sin^2\phi) sin^2\theta + a_z^2 cos^2\theta)^{\frac{3}{2}}} \quad (1)$$

with a_x, a_y and a_z the semi-axes of the ellipsoid (a_x>a_y>a_z), representing the anisotropic parameters. The scattered intensity as a function of ψ (angle in the detector plane) can therefore be written as (Bihannic et al., 2010) :

$$I(q,\psi) = C \int_0^{2\pi} \int_0^{\pi} F^2(q,\psi) PDF(\theta,\phi) d\theta d\phi \quad (2)$$

With C a constant, F(q,ψ) the platelet form factor, PDF(θ,ϕ) the probability density function of the normal vector, ψ the angle marking the angular variations of the 2D images, θ the polar angle and ϕ the azimuthal angle marking the platelet orientation. The angular variations of the scattered intensity of the 2D images are fitted with Equation

2 to extract the values of the anisotropic parameters. For this purpose, the scattered intensities are normalized by the average scattered intensity for angles between $\psi = 0$ and $\psi = 2\pi$. In addition, appropriate projections of the normal vector to the platelet from the shear frame of reference to the detector frame of reference are made to redefine the angles θ and ϕ as a function of the angle ψ (Bihannic et al., 2010). An example of the normalized intensity as a function of angle ψ at the radial and tangential positions for a 30 g/L 6-Cl gel with 0.15% in volume fraction of beidellite is given in Figure 4. The solid lines in Figure 4 represent the fit of the experimental data with Equation 2.

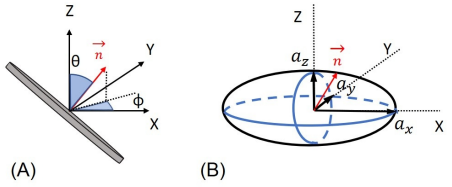

Figure 3: (A) Representation of the shear reference frame, in which the orientation of the vector normal to the platelet, $\vec{n}$, is depicted. (B) Ellipsoid showing the statistical confinement of the normal vector $\vec{n}$ of the clay platelet, featuring the anisotropic parameters a_x, a_y, a_z as the semi-axes of the ellipsoid ($a_x > a_y > a_z$) in the shear reference frame.

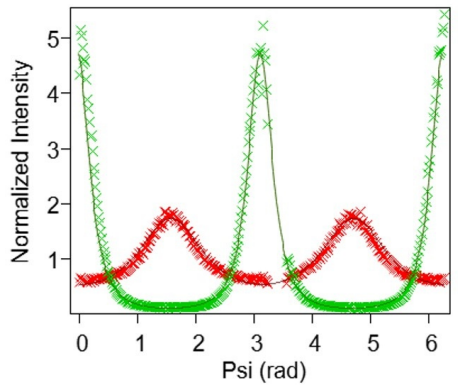

Figure 4: Normalized scattering intensity at q=0.03 Å^{-1} as a function of angle ψ for a 30 g/L 6-Cl gel with 0.15% BId-T3-Na under a shear of 3000 s^{-1}. In red: scattering intensity obtained in the radial position. In green: scattering intensity obtained in the tangential position. Crosses represent the experimental points and solid lines represent the fit of the experimental data with Equation 2.

Note that the anisotropic analysis in Figure 4 is best carried out at the maximum of clay-clay structure factor (i.e. peak arising due to the lamellar ordering of the clay platelets). For the data in Figure 4 this corresponds to q=0.03 Å^{-1}. It has been shown in the past (Van Der Beek et al., 2006), that for *plate-like* particles, we can indeed use the intensity variation of the platelet-platelet *structure factor* to obtain information about the orientation PDF of individual platelets. This would not be possible for example for *rod-like* particles. More precisely, it was shown that the anisotropy analysis, akin that in Figure 4, for *plate-like* particles can be done at *any* scattering wave-vector and would lead to the same results. It is however useful to perform the analysis at the position of the strongest peak in the signal (the first maximum in the platelet-platelet *structure factor*) in order to maximize the signal-to-noise ratio.

The ratios of anisotropic parameters a_z/a_y and a_y/a_x are obtained from the modelling of the curves in Figure 4 in the tangential and radial positions respectively. These anisotropic parameters allow us to then calculate the ratio of parameters a_z/a_x. The ratios a_z/a_x and a_y/a_x provide access to the motions shown in Figure 5 (A) and Figure 5 (B) respectively. Thus, a_z/a_x describes the rotation of the normal vector $\vec{n}$ around the Z axis in the plane ($\vec{\nabla V}$,$\vec{V}$) (Z being the direction perpendicular to the cross-sections depicted in Figure 5). The ratio a_y/a_x describes the rotation of the normal vector $\vec{n}$ around an axis parallel to $\vec{V}$ in the plane ($\vec{\nabla V}$,Z). These two ratios reach values between 0 and 1, where 0 corresponds to platelets being completely oriented in one direction and 1 corresponds to platelets being randomly oriented. The statistical confinement of the normal vector in this latter case describes a sphere (refer back to Figure 3).

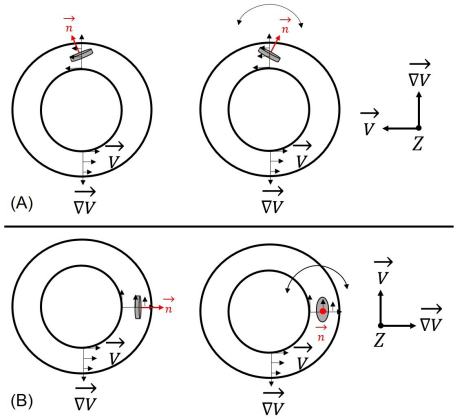

Figure 5: (A) Rotation of the normal vector $\vec{n}$ in the plane ($\vec{\nabla V}$,$\vec{V}$) around the axis Z as described by the ratio of anisotropic parameters a_z/a_x. (B) Rotation of the normal vector $\vec{n}$ in the plane ($\vec{\nabla V}$,Z) around the axis represented by $\vec{V}$ as described by the ratio of anisotropic parameters a_y/a_x.

3.2. Macroscopic behaviour under flow

We study the evolution of the viscosity of clay containing gels as a function of shear rate. Figure 6 (A) shows the evolution of viscosity as a function of shear rate for a 6-Cl hydrogel at 30 g/L for different volume fractions of the three clay types studied. A decrease in viscosity is observed with increasing shear rate. The gels thus exhibit a strong shear thinning behaviour. The decrease in viscosity η can therefore be described according to a power law

with the shear rate such as (Vigilato et al., 2015; Rahman et al., 2017; Kumbàr et al., 2017) :

$$\eta \sim K\dot{\gamma}^{n-1} \quad (3)$$

With K a constant in Pa.s^n corresponding to the consistency index and n a dimensionless number named rheofluidification index. If we take the example of the 30 g/L 6-Cl gel with 0.15% SAz1-T3-Na, we obtain a consistency value K = 24.5 Pa.s^n and a rheofluidification index n = 0.16 lower than 1, characteristic of a shear-thinning fluid. These values are similar regardless of the clay volume fraction for the 30 g/L ionene gel. Considering a

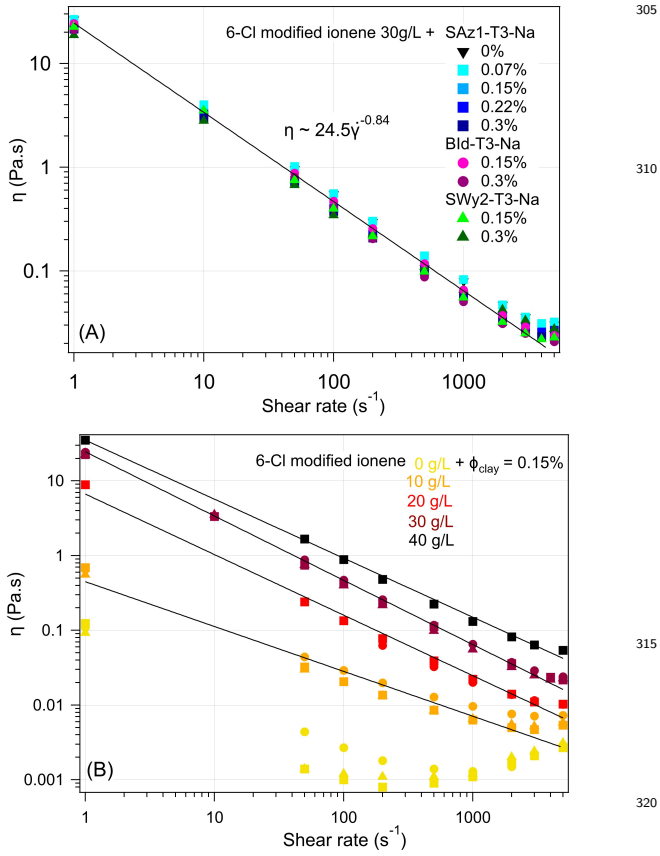

Figure 6: (A) Evolution of viscosity versus shear rate for 30 g/L 6-Cl gels for different clay volume fractions. The black solid line represents the power law fit of the experimental data for the 30 g/L 6-Cl gel and 0.15% SAz1-T3-Na. (B) Evolution of viscosity as a function of shear rate for gels with different concentrations of 6-Cl for a volume fraction of 0.15% clay and for the corresponding 0.15% clay suspensions. BId-T3-Na is represented by circles, SAz1-T3-Na by squares and SWy2-T3-Na by triangles. The black solid lines represent the power law fits of the experimental data.

10% uncertainty in the viscosity values, there are no significant changes in the hydrogel viscosity when platelets are added to the gel. Figure 6 (B) presents the evolution of the viscosity of the gels as a function of the shear rate for a volume fraction fixed at 0.15% in clay and for different 6-Cl concentrations. The viscosities of the corresponding clay suspensions at 0.15% are plotted in yellow in Figure 6 (B). We observe that the increase of the viscosity is mainly sensitive to the polyelectrolyte concentration. When we increase the concentration of 6-Cl from 10 g/L to 40 g/L, the viscosity of the gels increases by more than a factor 10. In Table 2 are listed the values of consistency K and rheofluidification index n for the gels at different concentrations of 6-Cl. We notice an increase of K when increasing the concentration of 6-Cl, which is expected since the K constant is directly related to viscosity. The rheofluidification index n decreases by a factor of 2 when increasing the concentration of 6-Cl from 10 g/L to 20 g/L. Then it appears to be almost constant. Thus, the shear-thinning behaviour of the gels is more pronounced for more concentrated gel rather than gels at the critical gelation concentration. Furthermore, it is observed at 6-Cl 10 g/L that the viscosity of the gel with BId-T3-Na at 0.15% is slightly higher than that of the gels with SWy2-T3-Na and SAz1-T3-Na at 0.15%. This is in agreement with previous studies (Hotton et al., 2021) specifying the fact that the highest G' value for these systems is also the one for the gel containing 0.15% beidellite. In the same way as for G', the differences in viscosity according to the nature of the clay seem to be visible only when the gel is close to the CGC.

Table 2: Values of K and n parameters and R^2 of the power law 3 for the 6-Cl hydrogels at different concentrations in ionene and 0.15% of clay.

	K (Pa.s^n)	n	R^2
6-Cl 10g/L	0.42	0.4	0.9967
6-Cl 20g/L	6.7	0.19	0.9998
6-Cl 30g/L	24.5	0.16	0.9999
6-Cl 40g/L	35	0.21	0.9999

The pure clay suspensions plotted in yellow on Figure 6 (B) present a very weak shear-thinning behaviour at the concentrations studied, with a nearly constant viscosity between 50 s^{-1} and 1000 s^{-1}. However, a slight increase of the viscosity is noticed at high shear rates from 2000 s^{-1}. This is characteristic of a Taylor-Couette instability (Philippe et al., 2012). This instability characterizes the appearance of secondary currents at very high shear rates. In the same way as for a low density gel, we also observe that the BId-T3-Na has a higher viscosity than the 0.15% montmorillonite suspensions. Overall, the shear-thinning behaviour of the system as well as its viscosity are essentially governed by the 6-Cl modified ionene.

3.3. Orientation of clay platelets inside the gel

The organisation of clay platelets at rest has been evidenced in our previous article, featuring a local lamellar order, with a repeat distance of roughly 20 nm, characterized by periodic modulations of the scattered intensity in the middle-q region (Hotton et al., 2021). As the planar platelet surface gives a q^{-2} dependence of I(q) vs q (the platelet form factor), the Kratky representation, q^{2}I(q), is the best to highlight the platelet-platelet correlations, i.e.

the structure factor. Figure 7 represents the evolution of the structure factor of the 6-Cl gel at 30g/L and 0.15% of SAz1-T3-Na between 5000 s^{-1} and 0 s^{-1} in tangential and radial positions. The same periodic oscillations compared to rest are observed under shear. We notice therefore that the interparticle distance and their periodic face-to-face organisation remains unchanged regardless of the shear rate. These observations are valid for all the other systems studied by rheo-SAXS in this article. We

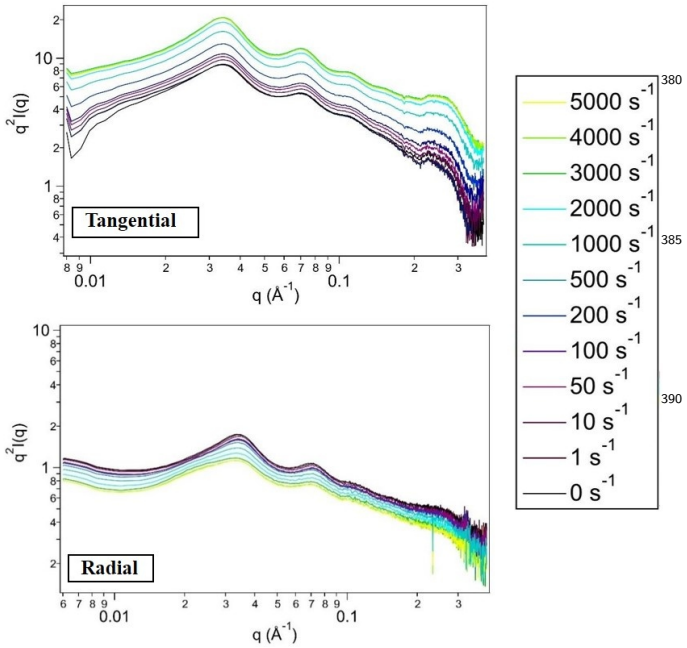

Figure 7: Evolution of the structure factor $q^2I(q)$ as a function of the scattering vector q for 6-Cl gel at 30 g/L and 0.15% of SAz1-T3-Na at different shear rates in the tangential and radial positions.

observe the appearance of an additional shoulder between 0.02 $Å^{-1}$ and 0.03 $Å^{-1}$ in the radial position. The origin of this shoulder remains unknown, however we know that it is the signal in the vertical sector of the 2D image that is responsible for it (see SI).

Since the scattering curves are different depending on whether one is placed parallel or perpendicular to the velocity lines, we can already state that the clay platelets are oriented under shear. To quantify this orientation, let us study the evolution of the two ratios of the anisotropic parameters as a function of the shear rate. To extract these parameters from the angular variations, we set the value of the scattering wavevector q at the first maximum of the oscillations, at around 0.03 $Å^{-1}$. We take this value in order to have the maximum of intensity.

Figure 8 shows the evolution of a_y/a_x and a_z/a_x as a function of the shear rate for 6-Cl gels at 30 g/L and at different volume fractions in clay. We first notice that both ratios are dependent on the shear rate from a critical shear rate of 50 s^{-1}. The ratio a_y/a_x is constant and close to 1 until 50 s^{-1}, and then decreases until 4000 s^{-1} from 1 to 0.85-0.75. Thus, the rotation of $\vec{n}$ in the plane ($\nabla\vec{V}$,Z) around the $\vec{V}$ axis (Figure 5 (B)) occurs quite freely regardless of the nature of the clay. The parameter a_z/a_x also begins to decrease from 50 s^{-1} until 4000 s^{-1} for values between 0.9 and 0.6 for both montmorillonites, and between 0.6 and 0.2 in the case of beidellite. The rotation of the normal vector to the platelet in the plane ($\nabla\vec{V}$,$\vec{V}$) around the Z axis (Figure 5 (A)) thus depends on the nature of the clay. For BId-T3-Na, a_z/a_x is close to 0.2 for shear rates above 3000 s^{-1} which means that the normal vector $\vec{n}$ is highly confined along the axis $\nabla\vec{V}$ and that its rotation in the plane ($\nabla\vec{V}$,$\vec{V}$) around the Z axis is minimal. There is no difference in orientation between SAz1-T3-Na and SWy2-T3-Na, both of them have a less confined normal vector along the $\nabla\vec{V}$ axis than that of BId-T3-Na in the plane ($\nabla\vec{V}$,$\vec{V}$). These trends are almost identical for different clay volume fraction. Thus, the orientation of the platelets is close to independent of the clay volume fraction at this polyelectrolyte concentration. We note that for hydrogels with beidellite particles, residual orientation is clearly seen at low shear rates. In other words the system does not relax completely to a non-oriented state, as the shear rate is decreased.

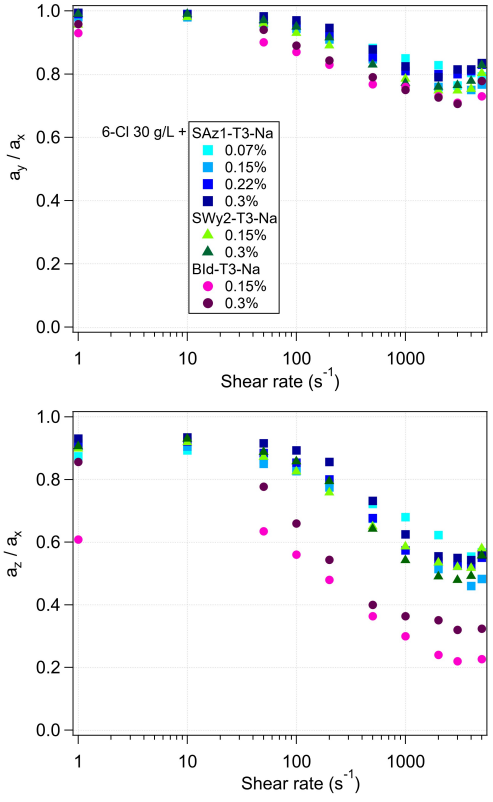

Figure 8: Evolution of the anisotropic parameters ratios a_y/a_x and a_z/a_x as a function of shear rate for 6-Cl gels at 30 g/L for different clay volume fractions. The same legend is used for both figures.

If the SAz1-T3-Na volume fraction is now set at 0.15% and the polyelectrolyte concentration varies from 20g/L

to 40 g/L, the same type of behaviour is observed in Figure 9. Orientation also takes place from a critical shear rate of 50 s^{-1}. The rotation of $\vec{n}$ in the plane ($\vec{\nabla V}$,Z) around the $\vec{V}$ axis occurs more readily, while the normal vector $\vec{n}$ is confined in the plane ($\vec{\nabla V}$,Z). Moreover, orientation is independent of the polyelectrolyte concentration in this range. The viscosity of the system, on the other hand, rises sharply with the polyelectrolyte concentration. Thus, platelet orientation is independent of the viscosity of the system. Furthermore, previous studies (Berry and Russel, 1987) have shown that the vicinity of particles with their neighbours improves platelet orientation. Thus, we would have expected that a decrease in interparticle distance i.e. an increase of the polyeletrolyte concentration would increase the degree of orientation, which is not the case here.

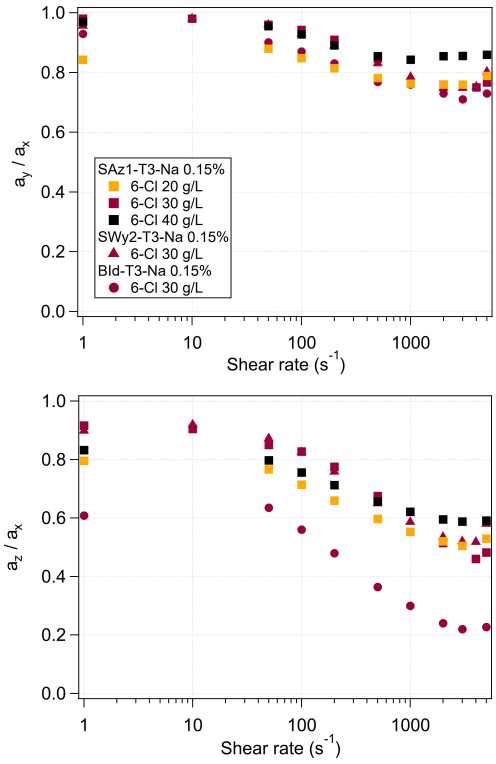

Figure 9: Evolution of the anisotropic parameters ratios a_y/a_x and a_z/a_x as a function of shear rate for 6-Cl gels at different concentration and with a clay volume fraction fixed at 0.15%. The same legend is used for both figures.

Figure 10 shows the evolution of anisotropic parameter ratios as a function of shear rate for 10 g/L 6-Cl gels with 0.15% of clay. The 10g/L system stands out from the other 6-Cl concentrations. In fact, when close to the CGC, we no longer observe a critical shear rate at which platelets orient themselves. Their orientation is then independent of the shear rate for both a_z/a_x and a_y/a_x. We demonstrate in the previous section that the 10 g/L gel is less shear-thinning than those between 20 g/L and 40 g/L in 6-Cl. Thus, dependence of shear rate on platelet orientation and shear-thinning behaviour of the gel are closely linked. A difference between SAz1-T3-Na and SWy2-T3-Na then emerged. Indeed, SWy2-T3-Na is the least oriented of the three clays with the highest a_y/a_x and a_z/a_x ratios. BId-T3-Na remains the platelets with the most confined normal vector in the plane ($\vec{\nabla V}$,Z) with the lowest a_z/a_x ratio. SAz1-T3-Na has an intermediate orientation between SWy2-T3-Na and BId-T3-Na with intermediate a_z/a_x values. In contrast, rotation of the normal vector around the $\vec{V}$ axis in the plane ($\vec{\nabla V}$,Z) occurs more freely for BId-T3-Na than for SAz1-T3-Na, the a_y/a_x ratio of beidellite being higher than that of SAz1. The clay with the most confined normal along $\vec{\nabla V}$ (beidellite) gives a gel with the highest viscosity. A low-density gel therefore emphasizes the differences in orientation depending on the nature of the clay. If we compare the system with 6-Cl 10 g/L and 0.3% of clay, where platelets are known to be aggregated within the gel (Hotton et al., 2021), there is a difference in platelet orientation compared with the 0.15% clay system (Supplementary Material). Both anisotropic parameter ratios are higher, so orientation is much lower. Thus, the presence of tactoids, i.e. the presence of a stack of platelets at short distances is detrimental to orientation. It is interesting to compare these results with previous work by Philippe et al. (Philippe et al., 2011) on the orientation under shear of clay platelets in suspension. In suspension, beidellite is also the system with platelets

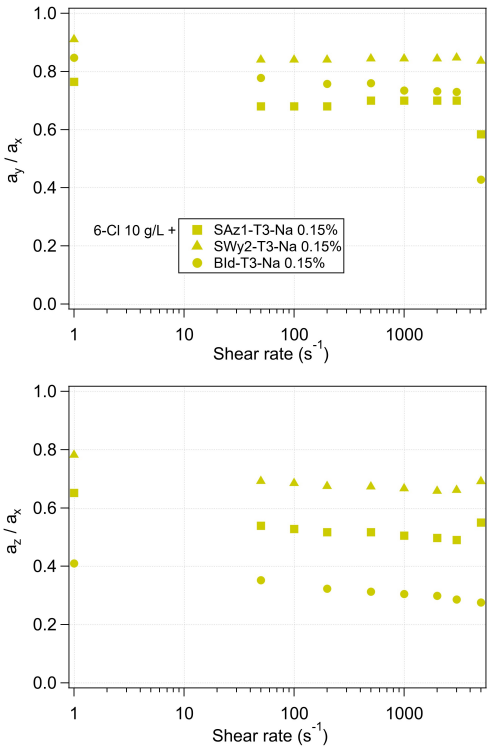

Figure 10: Evolution of the anisotropic parameters ratios a_y/a_x and a_z/a_x as a function of shear rate for 6-Cl gels at 10g/L and for 0.15% of clay volume fraction. The same legend is used for both figures.

having the most confined normal vector along the $\vec{\nabla V}$ axis compared to the two types of montmorillonite. SWy2 is also the clay that orientates the least under shear. So, although the system is different due to the presence of a dense meshwork of ionene polyelectrolytes, we find the same trends as in the case of pure clay gels or suspensions. Thus, it seems that platelet orientation is sensitive to charge location on the clay platelets. While beidellite has tetrahedral substitutions (thus charge located close to the surface of the platelets), montmorillonite has octahedral substitutions (charge located in the central part of the platelets). When the charge is located closer to the surface of the platelet, the degree of orientation is greater. The reason behind remains unclear. A possible link might be between *surface*, as opposed to central, charge location and a more significant *rigidity* of the clay platelets. The charge *density* of clays seems to have no effect, except for low-density gels with 10g/L of 6-Cl. In this case, higher charge density results in better platelet orientation. We have shown in a previous study (Hotton et al., 2021) that the degree of organisation of the clay platelets within the modified ionene gel depends as much on the location of the charge as on the charge density. As a consequence, the differences according to the nature of the clay are not reflected in the same way in their ability to orientate under shear than in the degree of platelet organisation.

4. Conclusion

These studies have shown the possibility to orientate clay platelets within the matrix of ionene-based gels under shear. The vector normal to the platelet is then essentially confined to the plane ($\vec{\nabla V}$,Z) during shear. Platelet orientation differs depending on whether the concentration of ionene in the gel is greater than or equal to the CGC. For ionene concentrations higher than the CGC, this orientation is independent of the clay volume fraction and independent of the ionene concentration. Thus, interparticle distance has no effect on platelet orientation. The orientation field is dependent on the shear rate and has a critical shear rate at which the platelets are oriented. The shear-thinning properties and viscosities of these systems are governed by the behaviour of the ionene. Thus, viscosity is decorrelated from the preferential orientation of the clay particles within the gel. When the concentration of ionene is equal to the CGC, the clay platelets exhibit an orientation independent of the shear rate. Regardless of the ionene concentration, orientation is essentially dependent on the nature of the platelet and, more specifically, on the location of the charge. On the other hand, the differences in charge density are only visible for ionene concentrations close to the CGC, i.e. for a weak gel network. In this case, the clay with the highest charge density is more oriented than the clay with the lowest charge density for the same charge location.

We note that while in this study all clay types orient in the same way under shear (albeit to a smaller or greater degree), other studies report completely different orientations under shear for montmorillonite and laponite clays, for example (Loizou et al., 2010). It is evident that the plethora of different clay platelets and their individual behaviour under shear, in the presence or absence of a polymer network, is far from being understood. For composite hydrogels, such as the present systems, it would be most instructive to couple both rheo-SAXS and rheo-SANS (Loizou et al., 2010), in order to understand the concurrent behaviour of the polymer and the clay nanoparticle component under shear.

The organisation of clays nanoplatelets in a local lamellar order paves the way to a promising material for drug delivery system with potentially anisotropic permeability. Indeed, a regular stacking of clay particles could lead to a tortuous diffusion pathway of the drug within the hydrogel. Morover the shear-induced orientation of clays opens the possibility to tune at will the anisotropy of permeation properties of the hydrogel. The orientation of clay particles within the hydrogel with other methods such as applying a magnetic field could be investigated.

Author contribution

CH was the main contributor to the study. CH, GD, JSP, TB, CG, PL, LM and NM performed experimental work. CH, GD, JSP, LM and NM jointly contributed to the design of the work. GD, JSP, LM and NM supervised the work. CH drafted the manuscript and the remaining authors contributed to its final version.

Declaration of Competing Interest

The authors declare that they have no known competing financial interests or personal relationships that could have appeared to influence the work reported in this paper.

Acknowledgments

The authors acknowledge the SOLEIL synchrotron for awarding the beamtime on beamline SWING. The authors acknowledge Adrian-Marie Philippe for the analysis tool for the SAXS data treatment.

Appendix A. Supplementary material

The Supplementary data to this article can be found at: Supplementary Material.pdf

References

Baravian C, Michot LJ, Paineau E, Bihannic I, Davidson P, Impéror-Clerc M, Belamie E, Levitz P. An effective geometrical approach to the structure of colloidal suspensions of very anisometric particles. EPL (Europhysics Letters) 2010;90(3):36005. doi:10.1209/0295-5075/90/36005.

Berry DH, Russel WB. The rheology of dilute suspensions of slender rods in weak flows. Journal of Fluid Mechanics 1987;180:475–494. doi:10.1017/S0022112087001915.

Bihannic I, Baravian C, Duval JF, Paineau E, Meneau F, Levitz P, de Silva JP, Davidson P, Michot LJ. Orientational order of colloidal disk shaped particles under shear flow conditions: a rheological-small-angle x-ray scattering study. The Journal of Physical Chemistry B 2010;114(49):16347–55.

Chang CW, van Spreeuwel A, Zhang C, Varghese S. Peg/clay nanocomposite hydrogel: a mechanically robust tissue engineering scaffold. Soft Matter 2010;6:5157–64. doi:10.1039/C0SM00067A.

Darvishi Z, Kabiri K, Zohuriaan-Mehr MJ, Morsali A. Nanocomposite super-swelling hydrogels with nanorod bentonite. Journal of Applied Polymer Science 2011;120(6):3453–9. doi:https://doi.org/10.1002/app.33417.

Davern JW, Hipwood L, Bray LJ, Meinert C, Klein TJ. Addition of Laponite to gelatin methacryloyl bioinks improves the rheological properties and printability to create mechanically tailorable cell culture matrices. APL Bioengineering 2024;8(1):016101. URL: https://pubs.aip.org/apb/article/8/1/016101/2932806/Addition-of-Laponite-to-gelatin-methacryloyl. doi:10.1063/5.0166206.

Hotton C, Ducouret G, Sirieix-Plénet J, Bizien T, Porcar L, Malikova N. Tuning structure and rheological properties of polyelectrolyte-based hydrogels through counterion-specific effects. Macromolecules 2023;56:923–33. doi:https://doi.org/10.1021/acs.macromol.2c01565.

Hotton C, Sirieix-Plénet J, Ducouret G, Bizien T, Chennevière A, Porcar L, Michot L, Malikova N. Organisation of clay nanoplatelets in a polyelectrolyte-based hydrogel. Journal of Colloid and Interface Science 2021;604:358–67. doi:https://doi.org/10.1016/j.jcis.2021.07.010.

Jeffery GB, Filon LNG. The motion of ellipsoidal particles immersed in a viscous fluid. Proceedings of the Royal Society of London Series A, Containing Papers of a Mathematical and Physical Character 1922;102(715):161–79. doi:10.1098/rspa.1922.0078.

Jesus CRN, Molina EF, Pulcinelli SH, Santilli CV. Highly controlled diffusion drug release from ureasil–poly(ethylene oxide)–na+–montmorillonite hybrid hydrogel nanocomposites. ACS Applied Materials & Interfaces 2018;10(22):19059–68. doi:10.1021/acsami.8b04559.

Kumbàr V, Š. Nedomovà , Pytel R, Kiliàn L, Buchar J. Study of rheology and friction factor of natural food hydrocolloid gels. Potravinarstvo Slovak Journal of Food Sciences 2017;11(1):203–209. doi:10.5219/735.

Leu Alexa R, Ianchis R, Savu D, Temelie M, Trica B, Serafim A, Vlasceanu GM, Alexandrescu E, Preda S, Iovu H. 3D Printing of Alginate-Natural Clay Hydrogel-Based Nanocomposites. Gels 2021;7(4):211. URL: https://www.mdpi.com/2310-2861/7/4/211. doi:10.3390/gels7040211.

Loizou E, Porcar L, Schexnailder P, Schmidt G, Butler P. Shear-Induced Nanometer and Micrometer Structural Responses in Nanocomposite Hydrogels. Macromolecules 2010;43(2):1041–9. URL: https://pubs.acs.org/doi/10.1021/ma9019448. doi:10.1021/ma9019448.

Michot LJ, Baravian C, Bihannic I, Maddi S, Moyne C, Duval JFL, Levitz P, Davidson P. Sol-Gel and Isotropic/Nematic Transitions in Aqueous Suspensions of Natural Nontronite Clay. Influence of Particle Anisotropy. 2. Gel Structure and Mechanical Properties. Langmuir 2009;25(1):127–39. doi:10.1021/la801894a.

Michot LJ, Bihannic I, Porsch K, Maddi S, Baravian C, Mougel J, Levitz P. Phase Diagrams of Wyoming Na-Montmorillonite Clay. Influence of Particle Anisotropy. Langmuir 2004;20(25):10829–37. doi:10.1021/la0489108.

Misawa Y, Koumura N, Matsumoto H, Tamaoki N, Yoshida M. Hydrogels Based on Surfactant-Free Ionene Polymers with N,N'-(p-Phenylene)dibenzamide Linkages. Macromolecules 2008;41(22):8841–6. doi:10.1021/ma801350k.

Murugesan S, Scheibel T. Copolymer/clay nanocomposites for biomedical applications. Advanced Functional Materials 2020;30(17):1908101. doi:https://doi.org/10.1002/adfm.201908101.

Noguchi R. Reactions of n,n,n',n'-tetramethyl–diaminoalkanes with dihaloalkanes. Macromolecules 1972;5(3):253–60.

Paineau E, Bihannic I, Baravian C, Philippe AM, Davidson P, Levitz P, Funari SS, Rochas C, Michot LJ. Aqueous Suspensions of Natural Swelling Clay Minerals. 1. Structure and Electrostatic Interactions. Langmuir 2011;27(9):5562–73. doi:10.1021/la2001255.

Philippe AM, Baravian C, Bezuglyy V, Angilella JR, Meneau F, Bihannic I, Michot LJ. Rheological Study of Two-Dimensional Very Anisometric Colloidal Particle Suspensions: From Shear-Induced Orientation to Viscous Dissipation. Langmuir 2013;29(17):5315–24. doi:10.1021/la400111w.

Philippe AM, Baravian C, Imperor-Clerc M, de Silva JP, Bihannic I, Davidson P, Meneau F, Levitz P, Michot LJ. Rheo-saxs investigation of shear-thinning behaviour of very anisometric repulsive disc-like clay suspensions. J Phys Condens Matter 2011;23(19):194112. doi:10.1088/0953-8984/23/19/194112.

Philippe AM, Baravian C, Jenny M, Meneau F, Michot LJ. Taylor-couette instability in anisotropic clay suspensions measured using small-angle x-ray scattering. Phys Rev Lett 2012;108:254501. doi:10.1103/PhysRevLett.108.254501.

Rahman MNA, Qader OAJA, Sukmasari S, Ismail AF, Doolaanea AA. Rheological characterization of different gelling polymers for dental gel formulation. J Pharm Sci 2017;9:8.

Sheikhi A, Afewerki S, Oklu R, Gaharwar AK, Khademhosseini A. Effect of ionic strength on shear-thinning nanoclay–polymer composite hydrogels. Biomater Sci 2018;6:2073–83. doi:10.1039/C8BM00469B.

Takeno H, Nagai S. Mechanical Properties and Structures of Clay-Polyelectrolyte Blend Hydrogels. Gels 2018;4(3):71. doi:10.3390/gels4030071.

Van Der Beek D, Petukhov AV, Davidson P, Ferré J, Jamet JP, Wensink HH, Vroege GJ, Bras W, Lekkerkerker HNW. Magnetic-field-induced orientational order in the isotropic phase of hard colloidal platelets. Physical Review E 2006;73(4):041402. URL: https://link.aps.org/doi/10.1103/PhysRevE.73.041402. doi:10.1103/PhysRevE.73.041402.

Vigilato MÁ, Horn M, Martins VCA, de G. Plepis AM. Rheological study of gels based on chitosan and carbon nanotubes. Brazilian Journal of Thermal Analysis 2015;4:35–8.

Yang Q, Miao Y, Luo J, Chen Y, Wang Y. Amyloid Fibril and Clay Nanosheet Dual-Nanoengineered DNA Dynamic Hydrogel for Vascularized Bone Regeneration. ACS Nano 2023;17(17):17131–47. URL: https://pubs.acs.org/doi/10.1021/acsnano.3c04816. doi:10.1021/acsnano.3c04816.

Zhao LZ, Zhou CH, Wang J, Tong DS, Yu WH, Wang H. Recent advances in clay mineral-containing nanocomposite hydrogels. Soft Matter 2015;11(48):9229–46. doi:10.1039/C5SM01277E.